UNIVERSITAT DE BARCELONA
Departament d'Astronomia i Meteorologia

UNIVERSITAT DE BARCELONA

Determination of the distance to the Andromeda Galaxy using variable stars

Memòria presentada per
Francesc Vilardell Sallés
per optar al grau de
Doctor en Física

Barcelona, gener de 2009

1 Introduction

1.1 The extragalactic distance ladder

Distance determinations are based on a hierarchic procedure where the closest distance indicators are used to calibrate farther distances. This process has been commonly known as the distance scale or the distance ladder, in the same way that the first rungs of a ladder are used to reach further steps. The first rung of the distance ladder is the Astronomical Unit, which can be determined by a wealth of different methods and procedures, either direct or indirect. With the determination of the Astronomical Unit and with accurate astrometric parallaxes, the distance to neighboring stars can be directly determined.

The most accurate and wide survey of astrometric parallaxes was obtained by the Hipparcos satellite (launched in 1989), which observed ~120 000 stars with an *absolute* parallax precision between 1 and 10 milliarcsec (Perryman & ESA, 1997; van Leeuwen, 2007). In the future, the Gaia mission is expected to greatly improve Hipparcos determinations, with a precision between 4 and 200 microarcsec for 10^9 stars (Perryman et al., 2001).

Geometric distance determination through parallaxes (with the exception of orbital parallaxes, see Herrnstein et al., 1999, as an example) is almost the only purely direct method. All the remaining distance determinations are based (to some extent) on the knowledge of the intrinsic luminosity of certain objects (usually referred as standard candles). Unfortunately, precise trigonometric parallax determinations (with errors below 10%) can only be obtained for the closest stars (~100 pc with Hipparcos). Therefore, as a new rung in the distance ladder, the trigonometric parallaxes are used to calibrate the luminosities of stars.

The number of photometric distance indicators is very large (see Jacoby et al., 1992, for a critical review), each one being suitable for certain distance intervals (Fig. 1.1). In all cases, the distance is obtained by knowing the intrinsic luminosity of the studied object (L_λ) at a certain wavelength λ and comparing it with the

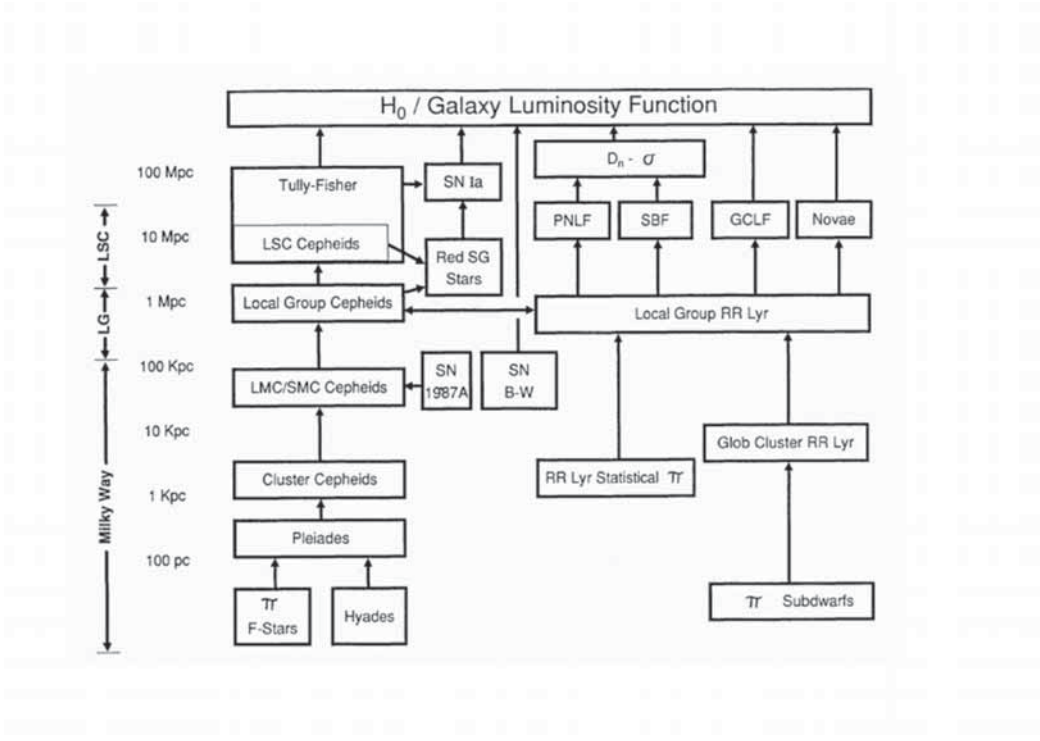

Figure 1.1. Distance determination techniques as described in Jacoby et al. (1992). The used abbreviations stand for: LSC — Local Super Cluster; SG — Supergiant; SN — Supernovae; B-W — Baade-Wesselink; PNLF — Planetary-Nebula Luminosity Function; SBF — Surface-Brightness Fluctuations; GCLF — Globular-Cluster Luminosity Function; π — astrometric parallax.

observed (absorption corrected) flux ($f^{\oplus}_{0,\lambda}$) through the expression known as the inverse square law of distance

$$f^{\oplus}_{0,\lambda} = \frac{L_\lambda}{4\pi d^2} \tag{1.1}$$

where d is the distance to the object of known luminosity. Equivalently, the distance can also be expressed in terms of the absolute magnitude (M_λ) of the object from the definition of the distance modulus

$$(m - M)_0 \equiv m_{0,\lambda} - M_\lambda = 5\log(d) - 5 \tag{1.2}$$

where $m_{0,\lambda}$ is the (absorption corrected) magnitude of an object at d parsecs.

Among all the standard candles, Cepheids play a central role in the distance ladder (Fig. 1.1). Cepheids are evolved variable stars (of spectral class F6 to K2) that pulsate radially (with periods ranging from ∼1 to ∼50 days). These variable stars have large amplitudes and bright intrinsic luminosities that make them easily detectable in photometric variability surveys, even in distant galaxies. In addition,

they present a strong correlation between the period of pulsation and their absolute magnitude (known as period-luminosity relationship, Leavitt & Pickering, 1912). The Cepheid period-luminosity (P-L) relationship has made of these variable stars one of the main cornerstones in deriving extragalactic distances (see Freedman et al., 2001, for a review).

The pulsation mechanism is relatively well understood from the theoretical point of view (see Gautschy & Saio, 1996, for a review). However, the large number of required assumptions has made that, in most cases, the calibration of the P-L relationship has been obtained empirically. The zero-point of the P-L relationship has been established from several distance indicators, such as the Hipparcos statistical parallaxes of Cepheids (Feast & Catchpole, 1997; Luri et al., 1998), from isochrone fitting to galactic open clusters and from the infrared surface brightness technique (Gieren et al., 1997). The slope of the P-L relationship has traditionally been obtained from extragalactic Cepheids. The largest effort in this sense has been performed by the OGLE group (Udalski et al., 1999), identifying $\sim$ 1300 Cepheids in the Large Magellanic Cloud (LMC).

The Large Magellanic Cloud has traditionally been used as the first extragalactic rung of the distance ladder because of its proximity to the Milky Way. However, its low metallicity and irregular geometry (see, i.e., Weinberg, 2000) has posed some doubts on the suitability of LMC as the first step of the extragalactic distance ladder, as illustrated by the large spread in distances (Fig 1.2) derived from different methods (Gibson, 2000).

Therefore, accurate distance measurements to other Local Group galaxies are crucial to calibrating the cosmic distance scale. Once Local Group galaxy distances are known, all of its various stellar populations are available as potential standard candles. As major rungs on the cosmic distance ladder, these galaxies serve as calibrators not only for Cepheids but also for novae, globular clusters, etc., reaching far beyond the bounds of the Local Group (Hodge, 1981). In addition, precise distance determinations to Local Group galaxies enable the calibration of cosmological distance determination methods, such as supernovae, Tully-Fisher relationship, surface brightness fluctuations, etc. A precise and accurate determination of the extragalactic distance ladder is crucial to understand the physics, the age and the size of the Universe.

1.2 The Andromeda Galaxy

The Andromeda galaxy (M 31) is the nearest external spiral galaxy (Sb; Hubble, 1929) and, with the Milky Way, one of the two largest galaxies in the Local Group. Since the pioneering work of Hubble (1929), a large variety of studies have been performed to investigate its structure and stellar content. A clear example of the structure of M 31 can be seen in Gordon et al. (2006), where infrared observa-

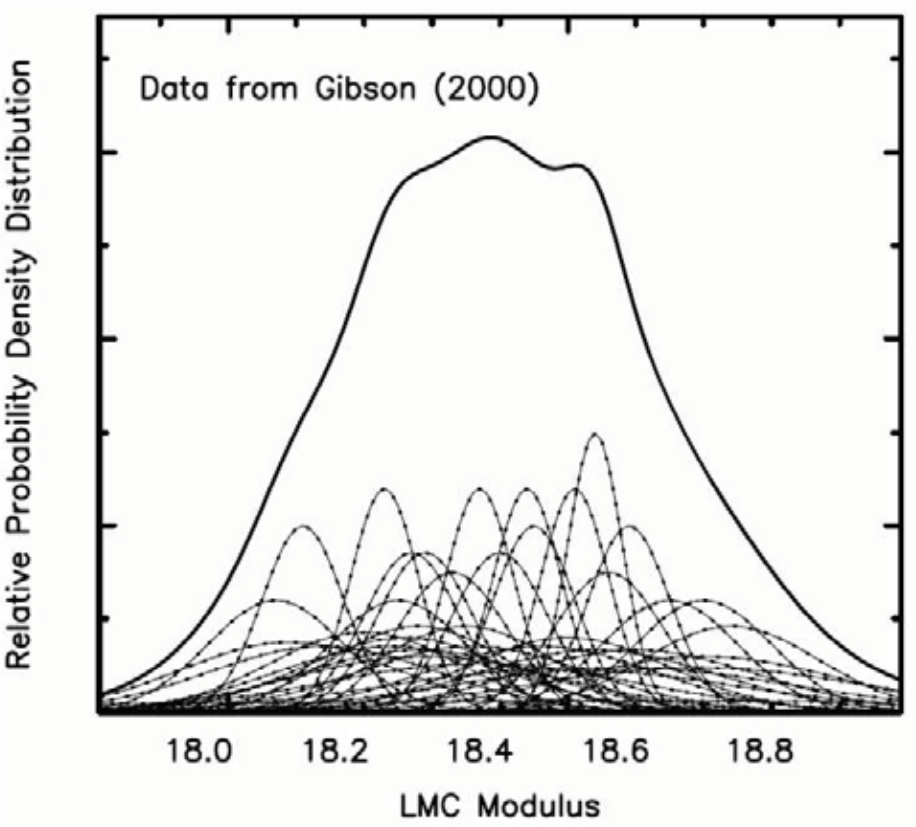

Figure 1.2. Frequentist probability density presented in Freedman et al. (2001); distribution of LMC distance moduli as compiled by Gibson (2000) plotted as a continuous probability density distribution built from the sum of individual unit-area Gaussians centered at the modulus in several works, and broadened by the published internal random error.

tions revealed its complex spiral structure, probably due to interactions with its numerous satellite galaxies. Other studies have revealed a rich stellar population (Massey, 2003) with all types of massive stars (e.g. main sequence stars, Wolf-Rayets, Luminous Blue Variable stars, Red Supergiants, etc). The analysis of its stellar population (and emission nebulae) has revealed that the metallicity of M 31 is very similar to that of the Milky Way. In addition, the similarity in size and morphology makes M 31 an ideal target to study spiral galaxy characteristics, allowing a better understanding of our own galaxy.

M 31 can also be a first-class distance calibrator (Clementini et al., 2001). On the one hand, and contrary to the Magellanic Clouds, the distance to M 31 is large enough so that its geometry does not introduce any systematics in the final distance determination. On the other hand, typically with a moderate reddening value ($E(B-V) = 0.16 \pm 0.01$, Massey et al., 1995), it is close enough to enable the individual identification of stars suitable for distance determination (such as

Cepheids). Moreover, an Sb I–II giant spiral galaxy (like M 31) provides a much more appropriate local counterpart for the galaxies commonly used for distance determination (e.g., Freedman et al., 2001). Finally, M 31 can also provide an absolute calibration of the Tully-Fisher relationship, enabling the calibration of the furthest distance determination methods. Therefore, although stars in M 31 are about six magnitudes fainter than those in LMC, the characteristics of this spiral galaxy make it a promising step of the cosmic distance scale.

Many studies have provided distance determinations to M 31 using a wide range of methods. A comprehensive list of distance determinations to M 31 are shown in Table 1.1 with explicit errors. As can be seen, the values listed are in the range $(m - M)_0$=24.0–24.6 mag. Most of the distance determinations in Table 1.1 rely on previous calibrations using stars in the Milky Way or the Magellanic Clouds. As a consequence of this, a large number of subsequent distance determinations, based only on recalibrations, can be found in the literature. These are not included in Table 1.1. The resulting weighted standard deviation is 0.08 mag (~4% in distance). As can be seen in Fig. 1.3 (where the range in distance modulus is the same that in Fig. 1.2), the dispersion is smaller than the dispersion in LMC distances, revealing that M 31 is potentially a better target to anchor the extragalactic distance scale. Therefore, a direct distance determination to M 31 (i.e., free from any prior calibrations) is of central importance to enable the use of this galaxy as the first step of the extragalactic distance ladder.

1.3 Eclipsing binaries

Eclipsing binaries (EBs) have always been an important tool for testing and determining the physical properties of stars (Popper, 1967; Guinan, 1993). They are composed of two stars that, when orbiting each other, produce periodic eclipses. The great potential of EBs is that their orbital motion, inferred from the radial velocity curves, and the shape of eclipses, obtained from the light curves, can be entirely explained by the gravitation laws and the geometry of the system (see Hilditch, 2001, for details).

Specifically, the light curves provide the relative properties and the orbital properties of the system (Table 1.2). The radial velocity curves can provide the systemic velocity (i.e., the velocity of the center of mass) and the velocity semi-amplitudes (i.e., the maximum velocity deviation of each component with respect to the systemic velocity). With these quantities, the semi-major axis of the system (a) and the individual mass of each component ($\mathcal{M}_P$, $\mathcal{M}_S$) can be determined from the following expressions (see Table 1.2 for nomenclature):

$$a \sin i = \frac{P(K_P + K_S)\sqrt{1 - e^2}}{2\pi} \tag{1.3}$$

Table 1.1. Distance determinations to M 31 as presented in the references. Values resulting from recalibrations of the same observational data, distance moduli without extinction corrections and distances derived in the present work are not included.

Method	$(m - M)_0$ [mag]	Distance [kpc]	Reference
Cepheids	24.20±0.14	690±40	[1]
Tip of the RGB	24.40±0.25	760±90	[2]
Cepheids	24.26±0.08	710±30	[3]
RR Lyrae	24.34±0.15	740±50	[4]
Novae	24.27±0.20	710±70	[5]
Cepheids	24.33±0.12	730±40	[6]
Cepheids	24.41±0.09	760±30	[6]
Cepheids	24.58±0.12	820±50	[6]
Carbon-rich stars	24.45±0.15	780±50	[7]
Cepheids	24.38±0.05	752±17	[8]
Carbon-rich stars	24.36±0.03	745±10	[8]
Glob. Clus. Lum. Func.	24.03±0.23	640±70	[9]
Red Giant Branch	24.47±0.07	780±30	[10]
Red Clump	24.47±0.06	780±20	[11]
Red Giant Branch	24.47±0.12	780±40	[12]
Cepheids	24.49±0.11	790±40	[13]
RR Lyrae	24.50±0.11	790±40	[14]
Tip of the RGB	24.47±0.07	785±25	[15]
Mean & std. deviation	24.39±0.08	750±30	

[1]: Baade & Swope (1963); [2]: Mould & Kristian (1986); [3]: Welch et al. (1986); [4]: Pritchet & van den Bergh (1987); [5]: Capaccioli et al. (1989); [6]: Freedman & Madore (1990); [7]: Richer et al. (1990); [8]: Brewer et al. (1995); [9]: Ostriker & Gnedin (1997); [10]: Holland (1998); [11]: Stanek & Garnavich (1998); [12]: Durrell et al. (2001); [13]: Joshi et al. (2003); [14]: Brown et al. (2004); [15]: McConnachie et al. (2005).

$$\mathcal{M}_P \sin^3 i = \frac{PK_S(K_P + K_S)^2(1 - e^2)^{3/2}}{2\pi G} \tag{1.4}$$

$$\mathcal{M}_S \sin^3 i = \frac{PK_P(K_P + K_S)^2(1 - e^2)^{3/2}}{2\pi G} \tag{1.5}$$

However, as can be seen from these equations, the inclination of the system, is needed for deriving the individual masses of the components and the semi-major axis. To obtain the inclination of the system, the light curves have to be modeled. The detailed modeling of the light curves involves a comprehensive understanding on the physical laws governing both the geometry of an EB system (usually de-

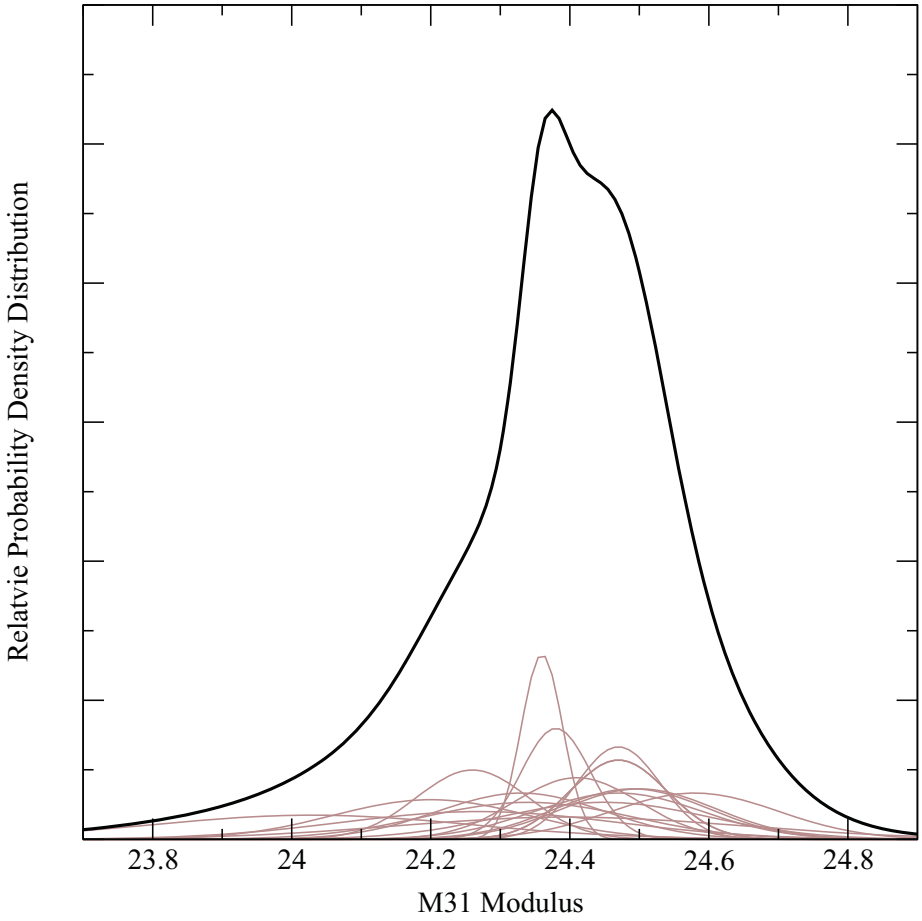

Figure 1.3. Distribution of M 31 distance moduli as compiled in Table 1.1 plotted as a continuous probability density distribution (black line) built from the sum of individual unit-area Gaussians centered at the quoted modulus, and broadened by the published internal random error (gray lines).

termined by the Roche lobe model) and the radiative properties of stars (including limb darkening, gravity brightening, reflection effects, etc.). The great number of processes involved in the light curve modeling has made that some specific algorithms, such as EBOP (Popper & Etzel, 1981) and the one by Wilson & Devinney (1971), have been developed to model the EB light curves. However, in all cases, the great number of involved parameters makes that expertise in modeling EBs is a necessary ingredient. In particular, the knowledge of possible correlations among parameters and the fundamental reasons for the observed correlations must be well understood to achieve an accurate solution. It is in this scenario when reducing the number of free parameters can be the proper way towards an accurate EB modeling.

In the course of the present work (Chap. 2 and Chap. 4), several assumptions are made to reduce the number of free parameters. The most important assumption

Table 1.2. EB properties that can be derived from different data sets. P and S stand for primary and secondary components, respectively, and a is the semi-major axis.

Parameter	Symbol	Light curves	Radial velocity curves	
			Single lines	Double lines
Period	P	✓	✓	✓
Eccentricity	e	✓	✓	✓
Argument of periastron	ω	✓	✓	✓
Luminosity ratio	L_λ^S/L_λ^P	✓	×	×
Inclination	i	✓	×	×
Radius of primary	R_P	$r_P = R_P/a$	×	×
Radius of secondary	R_S	$r_S = R_S/a$	×	×
Systemic velocity	γ	×	✓	✓
Semi-amplitude of primary	K_P	×	✓	✓
Semi-amplitude of secondary	K_S	×	×	✓

relates to the configuration of the system. In the Roche lobe model (see Hilditch, 2001, and references therein), the shapes of stars are determined by their surface potential. When the surface potential of a star is close to a certain limit (that depends basically on the mass ratio and the semi-major axis of the system), the star fills its Roche lobe. At this point, the surface layers of the star can flow out and accrete on the companion star. With this scenario, and depending on the value of the surface potential, the EB systems can be classified as (Fig. 1.4):

- Detached. Both stars are bound within separate equipotential surfaces. In this configuration the properties of every star are roughly independent on the presence of its companion.
- Semi-detached. Only one of the stars fills the Roche lobe (the companion is within a separate equipotential surface). In this configuration the shape of the component filling the Roche lobe is greatly distorted by the presence of its companion. In addition, the system can experience active mass transfer, implying that the evolution of both stars can depart from that of an isolated star.
- Over-contact. Both stars overfill their Roche lobes and share a common envelope. Therefore, their evolution and structure is closely coupled.

The adoption of a configuration can, therefore, reduce the number of free parameters. However, the final decision on the configuration adopted has to be well sustained by several indicators, including some tests with various possible configurations.

Another important consideration to accurately model an EB system is that, to

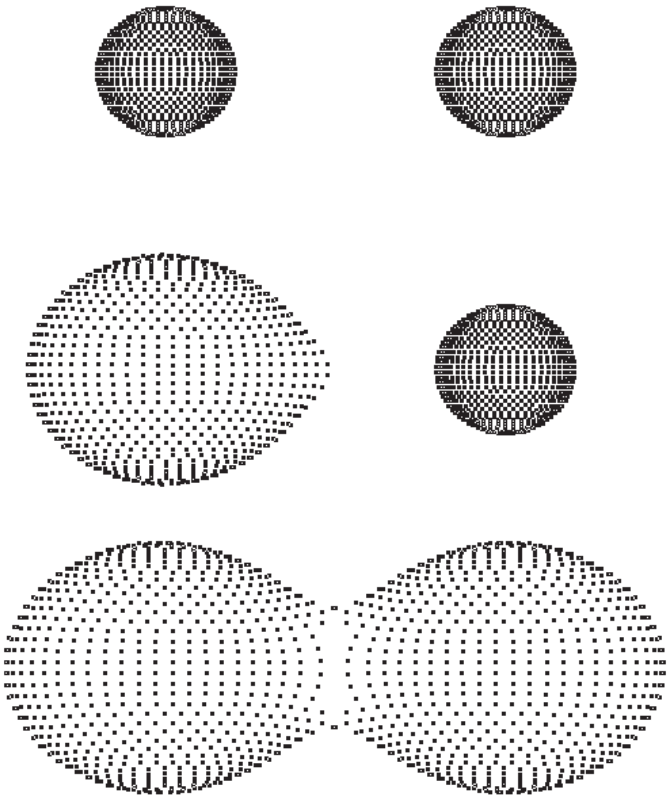

Figure 1.4. Diagram illustrating three possible configurations of an EB system. **Top:** Detached. **Middle:** Semi-detached. **Bottom:** Over-contact.

obtain the radial velocities, spectral lines have to be visible in the spectra. This leads to two possible scenarios:

- When the two components of the system have different luminosities and the lines of only one of them can be observed (called single-line binaries), the radial velocities can only provide the semi-amplitude of one of the components. In these systems, only a limited set of properties can be determined.
- When the luminosities of both components are similar, the spectroscopic lines of each component can be distinguished in the observed spectra. In these systems (called double-line binaries), all the orbital and physical quantities can be directly obtained (Table 1.2).

Therefore, for double-line EBs, the combination of light and radial velocity curves provides direct determinations of the individual radii and masses of the components without any prior calibration. However, a careful examination on the possi-

ble correlations and a detailed analysis of the minimum number of free parameters is required.

1.3.1 Distance determination methods

The direct determination of the radii (R) of the components of EB systems made that several authors (e.g., Lacy, 1977; Giménez et al., 1994) suggested the possibility to use EBs for deriving distances. The only additional requirement to determine the absolute luminosity of an EB system and, hence the distance, is the surface brightness (F_λ) or, equivalently, the effective temperature of the components ($T_{\rm eff}$).

The method of Lacy (1977) involves the use of the Barnes & Evans (1976) relationship to compute the surface brightness of the components. The distance modulus (Eq. 1.2) to each component is then computed assuming that the stars are roughly spherical ($L_\lambda = 4\pi R^2 F_\lambda$) through the expression

$$(m - M)_0 = m_\lambda - A_\lambda + 2.5 \log\left(\frac{R^2 F_\lambda}{R_\odot^2 F_{\lambda,\odot}}\right) - M_{\lambda,\odot} \tag{1.6}$$

with m_λ being the observed magnitude at a certain wavelength and A_λ being the line-of-sight absorption. In the equation above, the absolute magnitude ($M_\lambda = -2.5 \log(L_\lambda) + C_\lambda$) is expressed in terms of the solar properties ($R_\odot^2$, $F_{\lambda,\odot}$ and $M_{\lambda,\odot}$) to avoid numerical constants (C_λ).

Afterwards, Giménez et al. (1994) suggested the use of multi-band photometry and UV spectroscopy to better determine the temperature of each component. The distance modulus could then be computed from the definition of effective temperature

$$M_{\rm bol} = -2.5 \log\left(\frac{R^2 T_{\rm eff}^4}{R_\odot^2 T_{\rm eff,\odot}^4}\right) + M_{\rm bol,\odot} = M_\lambda + BC_\lambda \tag{1.7}$$

$$(m - M)_0 = m_\lambda - A_\lambda - M_{\rm bol,\odot} + 2.5 \log\left(\frac{R^2 T_{\rm eff}^4}{R_\odot^2 T_{\rm eff,\odot}^4}\right) + BC_\lambda \tag{1.8}$$

with BC_λ being the bolometric correction at a certain wavelength. The equation above is usually expressed for the V passband

$$(m - M)_0 = m_V - A_V - M_{\rm bol,\odot} + 5 \log\left(\frac{R}{R_\odot}\right) + 10 \log\left(\frac{T_{\rm eff}}{T_{\rm eff,\odot}}\right) + BC_V \tag{1.9}$$

and the absorption is usually determined from a color index (e.g., $(B-V)$) through the expression

$$A_V = \mathcal{R}_V E(B - V) = \mathcal{R}_V \left[(B - V) - (B - V)_0\right] \tag{1.10}$$

where $\mathcal{R}_V \equiv A_V/E(B-V)$ is the total-to-selective extinction ratio, usually assumed to be $\mathcal{R}_V = 3.1$ (e.g., Fitzpatrick, 1999).

The great advantage of this method with respect to other methods is that the required quantities can be obtained from the binary analysis (R) and from stellar atmosphere models ($T_{\rm eff}$, $(B-V)_0$ and BC_V). Therefore, no empirical calibration is needed to obtain the distance to the EB (calibrations to transform the stellar models into the above quantities are still required), making that the distance determination to any EB system is almost direct (Clausen, 2004). In addition, the luminosities of both components can be checked against the luminosity ratio derived from the light curve analysis (Table 1.2), resulting in a solution that is not only direct, but also auto-consistent.

1.3.2 The experience of LMC

The potential of EBs to derive distances, encouraged a project to obtain a direct distance determination to the LMC. The possibility to obtain ultraviolet to visible spectrophotometry (with the Hubble Space Telescope, HST) allowed the use of a specific temperature determination method. The spectrophotometric method is based on Eq. (1.1) and considers that the luminosity of a binary system (with components P and S) can be expressed as:

$$L_\lambda = 4\pi\left(R_P^2 k^P F_\lambda^P + R_S^2 k^S F_\lambda^S\right) \tag{1.11}$$

$$f_\lambda^\oplus = \left(\frac{R_P}{d}\right)^2 \left[k^P F_\lambda^P + k^S \left(\frac{R_S}{R_P}\right)^2 F_\lambda^S\right] 10^{-0.4A_\lambda} \tag{1.12}$$

where the absorption has been included. In order to consider the possibility that both components can be distorted by the presence of the companion star, a phase-dependent factor ($k^{P,S}$) has been introduced to consider the apparent size variations of the star (as seen from the Earth) and the reflection of light from the companion. Expressing the absorption in terms of the normalized extinction curve ($k(\lambda-V) \equiv E(\lambda-V)/E(B-V)$, Fitzpatrick, 1999) the equation above can be expressed as

$$f_\lambda^\oplus = \left(\frac{R_P}{d}\right)^2 \left[k^P F_\lambda^P + k^S \left(\frac{R_S}{R_P}\right)^2 F_\lambda^S\right] 10^{-0.4E(B-V)[k(\lambda-V)+\mathcal{R}_V]} \tag{1.13}$$

In the equation above, the surface fluxes $F_\lambda^{P,S}$ are obtained from atmosphere models. The distance is then calculated by finding the best fitting model spectra and normalized extinction curve to the spectrophotometry measured at the Earth ($f_\lambda^\oplus$).

Four EBs have been used up to now to determine accurate distances to the LMC using the method described above (Table 1.3). Light curves were obtained from previous photometric surveys using 1–1.5 m telescopes, and radial velocities

Table 1.3. Distance determinations to LMC as presented in Fitzpatrick et al. (2003). The two distances to LMC provided for each EB (depending on two different orientations of LMC) have been averaged.

System	d_{EB} [kpc]	d_{LMC} [kpc]	$(m-M)_{0,LMC}$ [mag]	Reference
HV 2274	47.0±2.2	46.5	18.3	[1],[2]
HV 982	50.2±1.2	50.7	18.5	[2]
EROS 1044	47.5±1.8	47.4	18.4	[3]
HV 5936	43.2±1.8	44.4	18.2	[4]
Weighted mean		48.3 ± 1.4	18.42 ± 0.06	

[1]: Guinan et al. (1998); [2]: Fitzpatrick et al. (2002); [3]: Ribas et al. (2002); [4]: Fitzpatrick et al. (2003).

were determined from medium-resolution spectra (R=15 500–23 000), obtained with Hubble Space Telescope (HST, 2.5 m) and Cerro Tololo Inter-american Observatory (CTIO, 4 m). Spectrophotometry was acquired with FOS and STIS instruments on board HST. The resulting distances have a scatter that is larger than their formal errors and seem to support the idea that the line-of-sight structure of the LMC is being detected and compromising its value as the first step of the extragalactic distance ladder.

1.3.3 Eclipsing binaries in M 31 and M 33

The first discoveries of M 31 EBs (~ 60 systems) came from photographic surveys in the 60's (Baade & Swope, 1965, and references therein). Due to selection effects, the observed binaries are among the brightest stars in the galaxy, being composed of luminous (and massive) O/B type stars. The low precision of the obtained light curves and the difficulty of obtaining radial velocities made that few attention was paid to these newly discovered EBs.

However, over the past two decades, the use of large format CCD detectors with high quantum efficiencies and low read-out noise has enabled the acquisition of precise (~ 0.01 mag) photometry for 19–20 mag stars with moderate size telescopes (2–3 meter). In addition, the development of improved reduction techniques (such as image subtraction, Alard & Lupton, 1998) has allowed the clear identification of EBs in galaxies well beyond the Local Group (e.g., Bonanos & Stanek, 2003). Together with the improvement on the quality of the light curves, large (8–10 m) telescopes have been built, enabling the acquisition of accurate radial velocities.

In this sense, the DIRECT group (see Macri, 2004, and references therein) started the identification of new EBs in M 31 (Fig. 1.5) and M 33, with 1.2–1.3

meter class telescopes, reporting almost 100 new EB systems in each galaxy. The resulting photometry has an error of $\sim$ 0.05 mag, which is just on the limit to disentangle the correlations among the parameters governing the light curve modeling. Even though, one of the detected EBs in M 33 was used to derive the first direct distance determination to M 33 (Bonanos et al., 2006).

1.4 Goals

Following the same principles already used for the LMC, **the fundamental goal of the present project is to carry out a one-step, accurate distance determination to M 31 using double-line EB systems** (Ribas & Jordi, 2003; Ribas et al., 2004). As previously mentioned (Sect. 1.3), the methodology involves, at least, two types of observations: photometry to obtain the light curves and spectroscopy to obtain the radial velocity curves.

Therefore, a large observational campaign was undertaken with the Isaac Newton Telescope (from 1999 to 2003) to find the most suitable EBs for distance determination to M 31. Following the DIRECT project, a field overlapping their observed fields (Fig. 1.5) was selected to obtain better quality light curves of their reported EBs. Observations were analyzed to discover eclipsing binaries and Cepheids suitable for distance determination (see Chap. 2).

Given the faintness of the targets, large telescopes (8–10 m) are needed to obtain the required radial velocities. The optimum targets for distance determination were selected to be observed with Gemini-North telescope (see Chap. 3). The resulting spectra were used to determine the fundamental properties for four of the selected EBs (Sect. 4).

The remaining needed parameters for distance determination (surface fluxes and line-of-sight extinction) can be obtained from several methods, either from modeling the spectral energy distribution or by new procedures (e.g., Sect 4.1.1.3). The combination of the results yields an accurate determination of the distance to the EB systems and, hence, to M 31 (Sect. 4.2).

In addition to providing accurate distances, the resulting fundamental stellar properties, such as masses and radii, can be used as powerful diagnostics for **studying the structure and evolution of stars that were born in a different chemical environment from that in the Milky Way** (Sect 4.1).

The large data volume treated also provides valuable information for the study of other stellar populations. As seen in previous sections, Cepheids are important standard candles. The photometric catalog resulting from the EB search yielded large numbers of Cepheids. Therefore, **the analysis of the Cepheid population was used to further constrain the distance to M 31** and enable the better calibration of the standard candles commonly used for distance determination (Chap. 5).

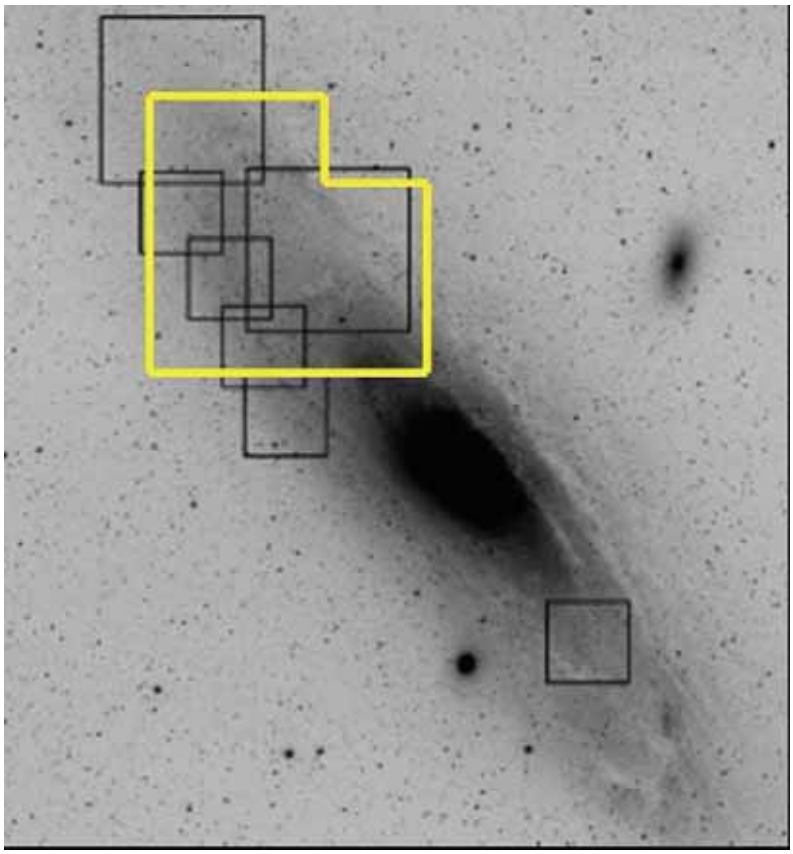

Figure 1.5. Image of M 31 as reported in Macri (2004) with the corresponding DIRECT fields (black boxes). The field studied in the present work has also been over-plotted (white box).

Finally, as a proof of the potential of the obtained photometric catalog and as a by-product of the present work, **the analysis of a flaring M star in the Milky Way**, revealed one of the most intense optical flares ever reported (Appendix A).